A Comparison of the Minimum Resolutions of Two Digital Image Correlation-Based Tools in Making Strain Measurements

Niranjan Desai, Purdue University Northwest; Christos Georgakis, Technical University of Denmark;
Gregor Fischer, Technical University of Denmark

Abstract

Structural health monitoring (SHM) is an important technique that helps structural engineers enhance the safety of critical structures and facilitates efficient maintenance of existing structures, while also assisting in the economic operation of the structure. SHM involves implementing a strategy that identifies and characterizes damage or undesirable performance in engineering structures. This investigation compared the minimum resolutions of two state-of-the-art digital image correlation-based software packages, ARAMIS and iMETRUM. The smallest strain accurately measurable using these tools was determined. This industry-affiliated study was performed in order to investigate initially undetected damage in the connections of the Storstrom Bridge in Denmark, whose detection would have prevented its propagation, resulting in lower repair costs.

Laboratory tests were performed on a specimen that modeled a steel beam-to-column connection of the bridge. In these tests, a shear force and bending moment were developed at the connection as it was loaded, and the corresponding strains that developed were measured using both conventional strain gauges as well as the two tools based on this digital image correlation (DIC). The minimum resolutions of both state-of-the-art systems used in this investigation were determined. Due to the challenges faced in making these small-strain measurements even under controlled laboratory conditions using ARAMIS, it was concluded that it would be unrealistic to use this tool in a real-world situation to measure strains as small as those that would need to be measured to detect the onset of damage in bridge connections.

The strains determined using iMETRUM were less sensitive to the presence of specimen vibrations produced by external perturbations in the vicinity of the specimen. Hence, to ascertain whether it is practical to use iMETRUM to measure small-strains in a real-world situation, more work needs to be done in making small-strain measurements using this tool in the presence of vibrations induced in the test specimen due to external disturbances.

Introduction

Structural health monitoring (SHM) is emerging as a vital tool to help civil engineers improve the safety and maintenance of critical structures and assists infrastructure owners with timely information for the continued safe and economic operation of their structures. SHM involves implementing a strategy that identifies and characterizes damage or undesirable performance in engineering structures. The conventional SHM process involves using global techniques that determine the health condition of structures by studying changes in their dynamic properties or responses. The system is observed over time by periodically sampling the dynamic response or deterioration obtained using an array of sensors. This is followed by extracting damage-sensitive features from these measurements and analyzing these features using statistical methods, thereby assessing the present condition (or current state of health) of the structure.

There also exist techniques to monitor the structural health at a local scale. Some of the techniques more commonly used on a local scale include the acoustic emission (AE) technique, the X-ray radiographic technique, and the interferometry technique [1-3]. A recent investigation of the condition of the Storstrom Bridge—which is a road and railway arch bridge, connecting Falster and Zealand in Denmark, and which is also on the rail line between Copenhagen, Denmark, and Hamburg, Germany—showed damage in local regions of the bridge (for example, the connections). On further investigation, it was inferred that this damage originated in regions of the connections hidden from the naked eye, such as behind gusset plates, and had propagated from there over time. The undetected damage in this bridge makes for an interesting and relevant situation that suggests that **local** structural damage may remain undetected using conventional SHM techniques that analyze changes in the global structural response parameters. Hence, this current study focused on applying a state-of-the-art DIC technique to monitor structural health, that is specifically applied to bridges, at a local level.

The goal of this investigation was to determine the minimum resolution of two state-of-the-art DIC systems by ascertaining the lowest possible strains that they are capable

of accurately measuring. The accuracy of the two systems in measuring small strains (strains in the range of 0.015% - 0.075%) was compared. It is important to know the minimum strain accurately measurable by a standard DIC-based SHM technique, so as to detect damage at its onset, thereby preventing it from spreading, as was observed in the case of the regions of the Storstrom connections that were hidden from external view. Since this investigation was motivated by connection damage in the Storstrom Bridge, the smallest strain accurately measurable using the DIC technique was determined by performing tests on a laboratory specimen that replicated a typical beam-column connection in the real bridge and computing the strains that developed in this connection using the DIC-based tools ARAMIS and iMETRUM.

This investigation expands upon an initial study that determined the accuracy of the DIC-based ARAMIS tool in measuring small-strains [4]. This investigation attempted to determine the accuracy of the DIC-based tool iMETRUM in making small-strain measurements of the same order of magnitude as those measured using ARAMIS, and also compared the accuracy of these two state-of-the-art tools. It was decided that iMETRUM would be used in the current investigation because, according to iMETRUM suppliers, iMETRUM is capable of overcoming many of the challenges faced in making small-strain measurements that were made using ARAMIS [4].

Background Work

As mentioned, the AE, the X-ray radiography, and the interferometry technique constitute some of the contemporary techniques used to monitor structural health on a local scale. Generally, it can be seen that the main challenges in applying these techniques are that they are expensive, labor-intensive, and involve having to make contact with the structure by placing sensors on it [1-3]. An alternative technique that can be used to monitor structural health involves the use of a photogrammetry system (using principles of image analysis and DIC), which applies a post-processing algorithm to analyze images of the structure captured during its loading phase, and computes the resulting strains and deformations in the structure [5, 6].

Photogrammetry is a non-contact measurement technology and has the following advantages [7]: it can be used to measure difficult-to-access structures; it has a fast measuring speed, and records large amounts of information in a short time by acquiring images; it is highly precise; it involves a simple process, and is less labor-intensive; and, it permits additional analysis of visual records at a later time.

Image analysis and DIC techniques involve first capturing a reference image of the object whose strains and deformations are to be measured. This represents the object in its undeformed state. As the object deforms, additional images are collected. The software package that is used to process these images recognizes the surface structure of the object and allocates coordinates to the image pixels. It compares the digital images and computes the object displacements and deformations. If the object surface has relatively few contrasting features or characteristics (homogenous surfaces), a stochastic color spray pattern is generally applied on the surface so that the different images can be compared and the strains and deformations computed [8]. Any random pattern can be used (for example, spray paint). However, the pattern must be such that there is an adequate contrast in the grayscale and surface pattern on the specimen surface [5, 6]. This can be achieved, for example, by using black and white spray paint to apply a random pattern on the surface of the object [5, 6].

The photogrammetry system captures the images during the loading process. Following this, it computes the deformation and the strain of the selected surface using a post-processing algorithm [5, 6]. There have been several successful applications of photogrammetry in the fields of aerospace engineering, chemistry, biology, architecture, and biomechanics, to name a few [7]. A non-contact photogrammetry system was used by Lin et al. [9] to measure the deformation of a pressure airship model. These structures are generally comprised of flexible materials, making them large and soft. Consequently, it is important to investigate the static and dynamic deformations of these structures in way that involves non-contact measurements.

Photogrammetry was used by Lee and Al-Mahaidi [10] to investigate the load-deformation characteristics of reinforced concrete T-beams ,strengthened with carbon fiber-reinforced polymer (CFRP) plates. Digital photogrammetry techniques were used to measure the vertical deflections of bridges by Jauregui et al. [11]. In all of the aforementioned cases, it was observed that the measurements obtained using the photogrammetry system showed a good correlation with experimental results and conventional measuring techniques. Also, Jauregui et al. [11] believe that photogrammetry in bridge engineering can provide an excellent alternative to conventional high-cost measurement systems. Close-range photogrammetry has not been as popular in bridge engineering applications as it has been in other areas [7]. Research activity on the application of this technique in bridge-related projects has been minimal and widely dispersed over the last 25 years [11]. However, there have been a few pioneering applications of the methodology applied in this field. There is a significant potential for growth in the

application of close-range photogrammetry in the field of bridge engineering. Additionally, the fast growth of digital imaging and computer technologies, the availability of inexpensive, off-the-shelf digital cameras, and soft-copy photogrammetry software systems has made more bridge engineering applications of photogrammetry involving deformation and geometry measurement a possibility [7].

On performing an overview of the cases involving the application of close-range photogrammetry to bridge engineering, it was observed that the field work for bridge geometry measurement has been reduced by more than 50%, while maintaining the same level of accuracy compared to conventional surveying methods [7]. It has also been found to be useful in historic bridge rehabilitation projects [7]. It can be concluded that close-range photogrammetry is a powerful, non-contact measurement technique that can provide unique solutions for a wide variety of bridge engineering applications [7]. There exist more recent applications of this technique in the field of bridge engineering. Waterfall et al. [12] looked at three case studies involving the application of DIC techniques towards obtaining measurements of bridges; namely, a post-tensioned concrete road bridge, a steel girder railway bridge, and a steel highway bridge. On completing these case studies, it was concluded that the measurements obtained using the advanced DIC system showed a good match with those obtained using conventional methods. Additionally, this technique makes it possible to measure large areas and several points, including inaccessible regions, efficiently, quickly, and in a cost-effective manner, making its implementation in industry more likely.

Recently, Busca et al. [13] compared several state-of-the-art vision-based measurement techniques (specifically, cameras) against traditional ones, by conducting tests on the response of an existing bridge during train transit. The goal of the research was to attempt to move from a 1D measurement at a single point, towards an approach where a single camera can obtain measurements in two or more points up to continuous measurement. It was observed that, for the single-point and multi-point measurements, the approach was promising, in that the limits in moving from single-point to two- and higher-point measurements were not that harsh. Also, a good representation of the dynamics of the system was obtained from the measurements, with the same limits of the displacement sensors. For the case of continuous measurement, an attempt was made to get the image of the complete structure using no targets at all, just working on the image contrast between the main beams and the background sky. It was concluded that the accuracy of the results obtained using this targetless approach was not as good as that obtained using targets. Yarnold et al. [14] implemented a comprehensive SHM system on the Tacony-Palmyra Bridge in Philadelphia, PA. The objective of the project was to preserve the structure using developments in SHM technology. The instrumentation used to monitor the structure included electrical resistance and vibrating wire strain gages, tilt sensors, a weather station, and cameras that were placed at selected locations along the structure. A live web portal and a customized playback program were used for the integration of the data and video. The live web portal permitted real-time viewing of the data and video over the Internet. The playback program allowed specified events, such as bascule openings and overloaded vehicular passage, recorded by the structural monitoring software, to be viewed. With the long-term SHM system in place, it has become possible to make important structural measurements, like maximum strain release during bascule openings and maximum strain variation due to vehicular overload. The structure's deformation response to loading and environmental effects was also developed.

Methodology

A typical beam-to-column moment connection of the Storstrom Bridge was replicated in the laboratory. A point load directed vertically downward was applied on the beam at an eccentricity from the connection at the column. This developed a shear force and bending moment at the connection, in a manner that occurred in the real-life joint. As the load was gradually increased over the course of the test, strains were measured at six different locations at the connection using the DIC-based ARAMIS and iMETRUM tools, as well as conventional strain gauges (described subsequently). These measurements were taken at the same instant of time, so as to enable a comparison between the readings obtained by the DIC-based approach and the conventional strain gauges. The accuracy of the strains obtained using the DIC approach were determined by comparing these values against those obtained using the conventional strain gauges. Finally, the lowest strains accurately measurable using both the DIC-based ARAMIS and iMETRUM tools were subsequently obtained.

Figure 1 shows the laboratory specimen that was designed by Furlan [15] and which was comprised of three steel S355/Fe510 plates (10 mm thick), a main plate (850 mm long by 150 mm wide), and two other plates, referred to as secondary plates (both of which were 300 mm long by 150 mm wide). One edge of each of the two secondary plates was bolted to an edge of the main plate via nine high-resistance bolts. This resulted in the edge of the main plate being sandwiched between the two secondary plates. The other end of each of the two secondary plates was welded to a fixed plate, which was bolted to a support that held the entire system in place. The junction at which the edge of the main plate was sandwiched between the edges of the two

secondary plates represented a typical beam-to-column bolted connection, with the main plate representing a beam. From here on, the region where the main plate is sandwiched between the two secondary plates using bolts will be referred to as the connection. Additionally, the other end of the main plate (or beam) was left free, and the external point load was applied vertically downward at this location during the test.

Figure 1. Laboratory Specimen (Adapted From Furlan [15]) Note. From "Use of Digital Image Correlation for Steel Strain Section Evaluation," by M. Furlan, 2014, unpublished master's thesis, Technical University of Denmark. All images reprinted with permission.

The connection was designed by Furlan [15] in accordance with the Eurocode 3 (EC3) provisions. It was comprised of nine high-resistance bolts of class 8.8. This configuration ensured that the stress in the bolts remained below their yield stress. Consequently, the bolts were in the same initial condition every time the test was repeated. The load was applied at the free end of the beam using a mechanical setup. A hydraulic jack was also available as another option. While being easier to use, it was harder to control than the mechanical setup over the low range of loading being applied in this experiment (a maximum load of 13.10 kN was applied). Furthermore, the vibrations created by the mechanical setup were less than those caused by the hydraulic jack. Vibrations led to noise in the experimental output (strain-versus-load diagram), which was undesirable. Using the mechanical setup, the load was manually increased by incrementing its value in a stepwise manner. The load cell was calibrated and the load values, which were read in mV, were converted to the corresponding values in kN. The process used to calibrate the load cell is described in the next subsection. The specimen was loaded to 70% of its yield stress. This ensured that it remained undamaged over the entire course of the test, and was in the same condition every time the test was repeated. The value of the loading that caused the specimen to be at 70% of its yield stress was determined by Furlan [15]. He developed a complex finite element model that incorporated the essential characteristics of the real specimen, using the ABAQUS software package. He concluded that the specimen yielded at 18.71 kN. Hence, in the current test, the specimen was loaded in increments to a maximum load of 0.7*18.71 = 13.1 kN

The load cell needed to be calibrated, since its output was in the form of voltage (in units of mV), which needed to be converted to equivalent units of force (kN). The load cell was calibrated by progressively loading it in five increments of 2.5 kN and one increment of 0.75 kN, noting the corresponding output voltage readings in mV. Thus, the load cell was loaded to a final value of 13.25 kN, which was slightly greater than the maximum value of load applied to the specimen during the tests (13.1 kN). These readings were plotted to develop a graph of load in kN (y-axis) versus voltage in mV (x-axis). Figure 2 shows this plot, which is linear, since the specimen was in its elastic region of response. Based on this calibration, the following linear relationship was obtained that was subsequently used to convert the load-cell voltage output in mV into an equivalent value of force in kN:

$$Force(kN) = \left[5780 * voltage(mV)\right] + 39.877$$

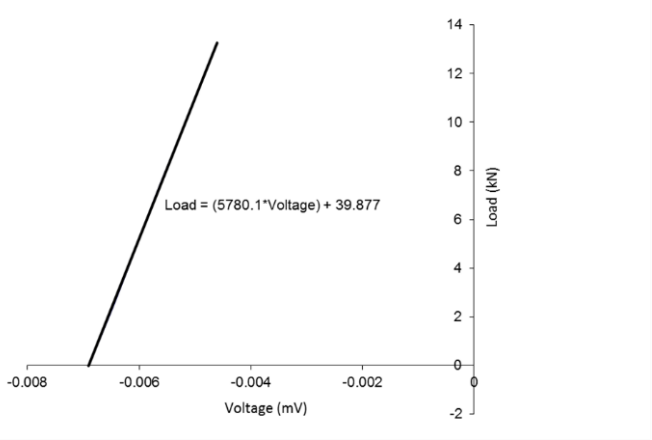

Figure 2. Calibration of the Load Cell

As the specimen was loaded, strains were measured at six locations in the connection at which high-stress variations were observed. These locations were determined by Furlan [15] and based on the results he obtained during his ABAQUS-based finite element model analysis of the specimen. These strains were measured using both conventional strain gauges as well as DIC-based techniques. The strain gauge readings obtained were used as a reliable reference to which the strains measured by the DIC-based approach

were compared, and their accuracy determined. In order to accomplish this task, six strain gauges were attached on the same face of the specimen at the connection (see Figure 3): three were attached to the outer surface of one of the secondary plates at the connection, and the remaining three were attached to the main plate. Digital images were captured of the opposite face of the connection on which the strain gauges were placed, thereby enabling the computation of strains in hidden regions. On both the main plate and the secondary plate in the connection region, the locations at which the strain gauges were attached were selected so as to include the following regions:

- A region in which tensile strain in the main plate (beam) develops. Hence, one strain gauge was placed near the top (upper) edge of the beam, where the tensile strain was maximum.
- A region in which a compressive strain in the beam develops. Hence, one strain gauge was placed near the bottom (lower) edge of the beam, where the compressive strain was maximum.
- A region in the beam (within the connection region) very close to the neutral axis, where the value of strain was minimum.
- A region in which tensile strain in the secondary plate develops. Hence, one strain gauge was placed near the top (upper) edge of the secondary plate in the connection, where the tensile strain was maximum.
- A region in which a compressive strain in the secondary plate develops. Hence, one strain gauge was placed near the bottom (lower) edge of the secondary plate at the connection, where the compressive strain was maximum.
- A region in the secondary plate (within the connection region) very close to the neutral axis, where the value of strain was minimum.

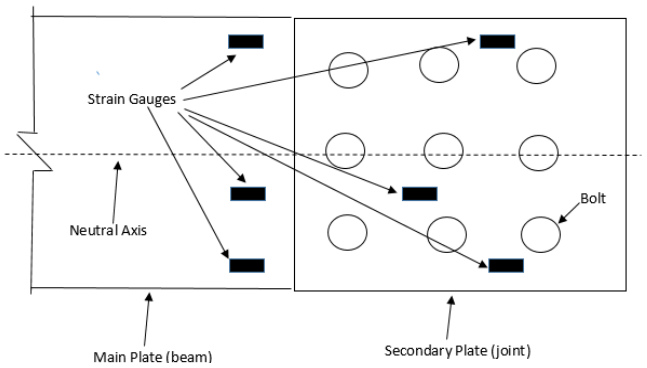

Figure 3. Location of the Strain Gauges

At the connection, the strains developed in the secondary plates were much smaller than those developed in the main plate (beam), because, in the former case, there were three plates bolted together, while, in the latter case, there was only one plate. Hence, this positioning of strain gauges provided a wide range of strain measurements in different regions of the connection: a) maximum connection tensile strains in both the beam (main plate) and the connection (secondary plates), the strains in the secondary plate being of a significantly lower value; b) maximum connection compressive strains in both the beam and the secondary plates at the connection, the strains in the secondary plate being of a significantly lower value; c) minimum connection strain values near the neutral axis, in both the beam as well as the secondary plate, the strain in the secondary plate being significantly lower than that in the beam.

Like the load cell output, the strain gauge output readings were also in mV. Consequently, the strain gauges were also calibrated in order to convert the output mV readings into their equivalent readings in units of strain (length/length). Traditional electrical resistance strain gauges provided by the laboratory that had a gauge factor, k, of 2.13 were used. For a single active gauge and three dummy resistors in a Wheatstone bridge configuration, strain was related to the output voltage (mV), gauge factor, and input voltage (5 mV) as follows: strain = [(4*output voltage)/(k*input voltage)]

Strain Measurement Using the DIC-Based Approach

As described earlier, the strains that developed in the specimen were measured using both traditional strain gauges (to provide a reference for comparison) and a DIC-based approach, using both the ARAMIS and iMETRUM DIC-based tools. The readings using the latter approach were compared against those obtained using the former. In order to make strain measurements using ARAMIS, digital images of the specimen were captured as it deformed under a progressively increasing load using a Nikon D800 digital camera (see Figure 4), supported by a tripod stand (see Figure 5). These images served as the raw data that was processed by the ARAMIS DIC-based algorithms to determine the specimen strain.

In order to make strain measurements using iMETRUM, a video of the specimen was captured as it deformed under a progressively increasing load using a GigE PoE camera (specifications: frame rate = 15 fps, resolution = 2452 x 2056 pixels) supported by a tripod stand. The video served as the raw data that was processed by the iMETRUM DIC-based algorithms to determine the specimen strain. This camera was recommended by the iMETRUM supplier for the strain magnitudes being measured in this test.

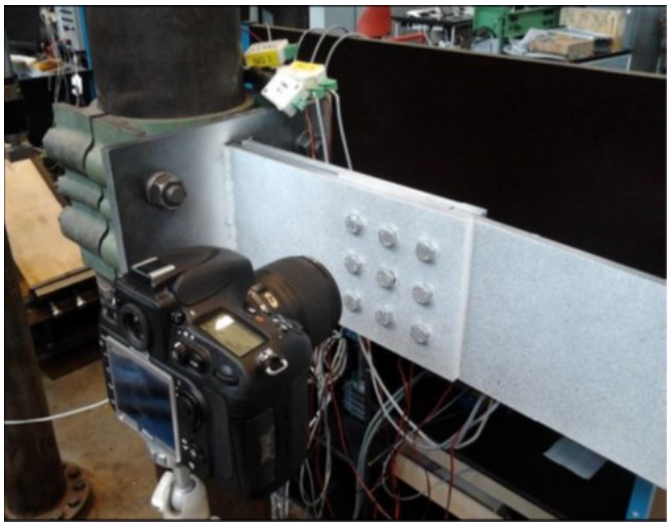

Figure 4. Placement of the Camera Relative to the Specimen (Adapted From Furlan [15])

Figure 5. Tripod Stand Used to Support the Camera (Adapted From Furlan [15])

The following parameters influenced the accuracy of the strains measured (relative to the strain gauge readings) on post-processing the digital images of the specimen:

- The focal length of the camera lens: While making the strain measurements using ARAMIS, three lenses with focal lengths of 24 mm, 60 mm, and 105 mm were used; the best results were obtained using the lens with the 60 mm focal length. A 60 mm lens was also recommended by Furlan [15] for this application. The iMETRUM supplier recommended and provided a high-resolution, low-distortion lens, having a focal length 35 mm, for the strain magnitudes being measured in this test. Hence, this lens was utilized.
- The distance of the camera from the face of the specimen: Another important parameter that influenced the quality of the output readings was the distance of the camera from the face of the connection. Each location of the specimen to which a strain gauge was attached was captured by the camera in isolation. Initially, it was attempted to capture all six locations at once. However, in order to accomplish this, the camera needed to be placed at a distance further away from the specimen than the optimum distance (see next paragraph) that gave the best readings. By doing so, the strains obtained on post-processing the images were inaccurate, showed a significant amount of noise, and did not compare well with the strain gauge readings. This was because the values of strain being measured in this experiment were very low and the camera had to be placed as close to the specimen as possible in order to accurately capture these values without losing focus of the specimen. Another issue with focusing on all six strain gauges in one picture was that the two plates of the connection that the camera was digitally capturing did not lie in the same plane, thus it was not possible to bring them both into focus in the same image.

Due to the very small values of strain being measured in this experiment, it was necessary to place the camera close to the face of the connection. In order to find the optimum value for this distance, several tests were performed by placing the camera at distances ranging from 7.5 to 20 cm from the face of the connection. Based on the test results, it was found that a distance of 10 cm from the face of the connection gave optimum results. At distances greater than this value, the strain readings obtained after post-processing the images were inaccurate in comparison to the traditional strain gauge readings that were used as a benchmark. At distances less than 10 cm from the connection face, it was not possible to bring the specimen into focus. A value of 10 cm was also recommended by Furlan [15] in order to obtain good results. An automatic focus camera was used in the ARAMIS tests.

While making the measurements using iMETRUM, the surface of the lens was placed at approximately 28 cm from the face of the specimen. This is a standard distance recommended by the supplier for the magnitude of strain being measured. Unlike the case of the ARAMIS camera, the iMETRUM camera did not focus on the specimen automati-

cally. In order to bring the specimen into focus, the technique recommended by the iMETRUM supplier was used. Placing the lens 28 cm away from the specimen surface, any external light source illuminating the specimen was turned off and the specimen was exposed only to the ambient light in the laboratory. Under these conditions, the camera shutter was completely opened. Now, the specimen surface was viewed through the camera. The surface appeared blurry and unfocused. The lens was gradually moved back and forth by a short distance (falling within about 5 cm) until the specimen surface came into focus.

- The spray pattern applied across the specimen surface: ARAMIS and iMETRUM process the digital images captured during the test by tracking the movement of single pixels and comparing the successive photographs obtained at each stage of loading. In order for the software to perform this task, it is essential that there be an adequate contrast in the grayscale and surface pattern on the specimen surface. Figures 6 and 7 show the final spray patterns used in two locations. These helped the researchers to visualize the spray pattern used. This was accomplished by using two different colors—a uniform white background on the specimen surface to conceal any imperfections on its surface, and a black spray that was discontinuously applied over the white background. This created black points whose displacements could be tracked by the software algorithm. Furlan [15] investigated the effect of the spray pattern on the accuracy of the results and, after trying several different patterns, observed that the use of a finer pattern led to more accurate results. Consequently, Furlan's pattern was used in this investigation.

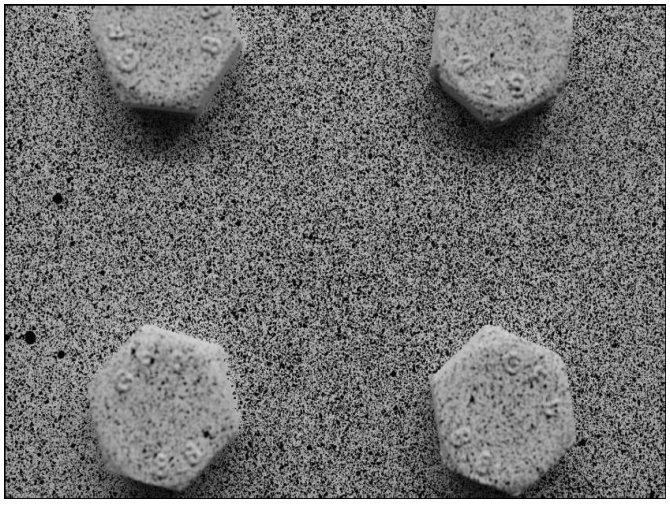

Figure 6. Final Spray Pattern—Joint Middle, Adapted From Furlan [15]

Figure 7. Final Spray Pattern—Joint Bottom, Adapted From Furlan [15]

- The existence of external vibrations while conducting the test: The camera was programmed to automatically capture an image every 45 seconds. Durations of 30 seconds, 60 seconds, and 75 seconds were also tried. It was observed that 45 seconds was an optimum time interval, since it was long enough to give the specimen enough time to settle after each manually applied load increment, yet of an appropriate duration to complete the experiment in a reasonable amount of time. Furthermore, programming the camera to automatically capture the images circumvented the need to make contact with the camera manually to capture each image. The experiment was extremely sensitive to vibrations, and even small perturbations caused by the most delicate of physical contact with the sensor created noise in the output readings. iMETRUM was less sensitive than ARAMIS to vibrations in the test specimen. iMETRUM made a continuous video recording of the deformation of the specimen as it was being loaded. This video recording served as the raw data that was processed by the DIC algorithms incorporated in the iMETRUM software. Vibrations existing in the specimen were captured in the video recording. While processing the video recording, the iMETRUM algorithms filtered out the noise created by the specimen vibrations.
- The lighting: While performing the strain measurements using ARAMIS, the specimen surface being digitally captured was brightly illuminated using two external light sources, in addition to any ambient light that already existed in the laboratory. In order to obtain accurate readings, it was important to ensure that the entire surface of the connection was uniformly illuminated and there were no shadows from nearby objects. An LED panel light and stand were pro-

vided by the suppliers of iMETRUM. Moderate illumination uniformly applied across the specimen surface, about as intense as the ambient light, was adequate for the iMETRUM measurements.

- The relative orientation of the specimen and lens faces: In order to obtain accurate readings, it was essential that the face of the camera lens be oriented parallel to the face of the connection being photographed. This was accomplished using a built-in feature of the digital camera, such that when viewed through the camera, the region of the specimen in focus was covered with red squares. A high concentration of red squares across the surface meant that the specimen surface in focus was parallel to the camera. A sparse concentration of red squares across the specimen surface implied that the camera position required adjustment in order to ensure that it was parallel to the specimen surface. In the case of iMETRUM, the lens surface was manually placed approximately parallel to the specimen face. A slight relative inclination between the two surfaces did not affect the accuracy of the strains measured using iMETRUM, since its algorithms were designed to account for this.

Several tests were conducted at each strain gauge location, and the strains obtained using ARAMIS and iMETRUM were compared with those obtained using traditional strain gauges at each location of the specimen under scrutiny. In order to be concise, only representative results at each location are presented. To save space, more than one set of resulting plots are presented at only the middle of the joint, where results are shown from two different tests. This was the stiffest part of the specimen and the strains here were consequently the lowest, thereby reaching the limits of the DIC-based techniques in measuring strains.

Analysis and Results

Figures 8-14 show comparisons between the strains measured using the DIC-based tools, ARAMIS and iMETRUM, and those measured using the traditional strain gauges. Table 1 shows the peak strain measured using ARAMIS, iMETRUM, and the strain gauges at the six locations investigated. Table 2 shows the percentage change between these peak strain values and those measured using the strain gauge value as the reference value.

Table 1. Peak Strains Measured using the DIC-Based Approach

Location	Strain (%): ARAMIS		Strain (%): iMETRUM		Strain (%): Strain Gauge		Type
Joint Middle	Test 1: 0.027	Test 2: 0.0116	Test 1: 0.022	Test 2: 0.0212	Test 1: 0.0149	Test 2: 0.0145	Compressive
Beam Middle	0.0245		0.0285		0.0264		Compressive
Joint Bottom	0.0298		0.03		0.0309		Compressive
Joint Top	0.0255		0.0299		0.029		Tensile
Beam Bottom	0.0723		0.0725		0.072		Compressive
Beam Top	0.0725		0.0745		0.073		Tensile

Table 2. Percentage Change between Peak DIC-Strains, Relative to the Strain Gauges

Location	% Change ARAMIS		% Change iMETRUM	
Joint Middle	Test 1: 44.82 (+*)	Test 2: 25 (-*)	Test 1: 47.65 (+)	Test 2: 46.21 (+)
Beam Middle	7.2 (-)		7.95 (+)	
Joint Bottom	3.56 (-)		2.91 (-)	
Joint Top	12.07 (-)		3.1 (+)	
Beam Bottom	0.41 (+)		0.69 (+)	
Beam Top	0.685 (-)		2.055 (+)	

* (+/-) = increase/decrease relative to strain gauge value

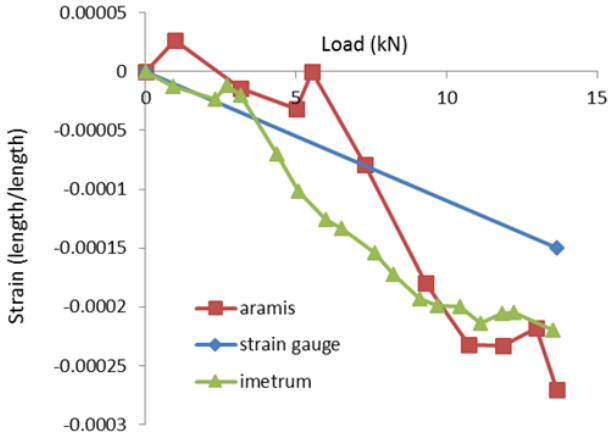

Figure 8. Comparison of Strains in the Middle of the Joint (Test 1)

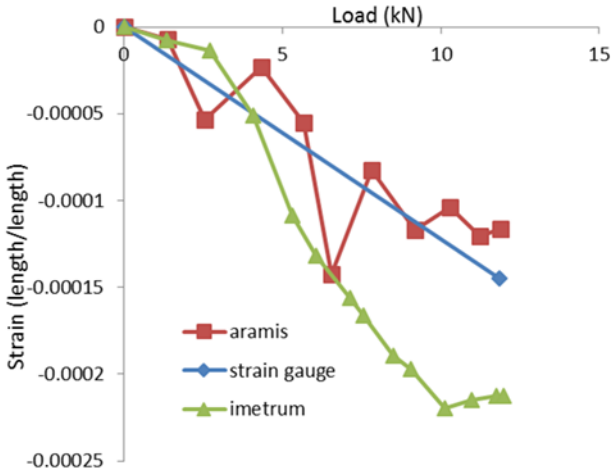

Figure 9. Comparison of Strains in the Middle of the Joint (Test 2)

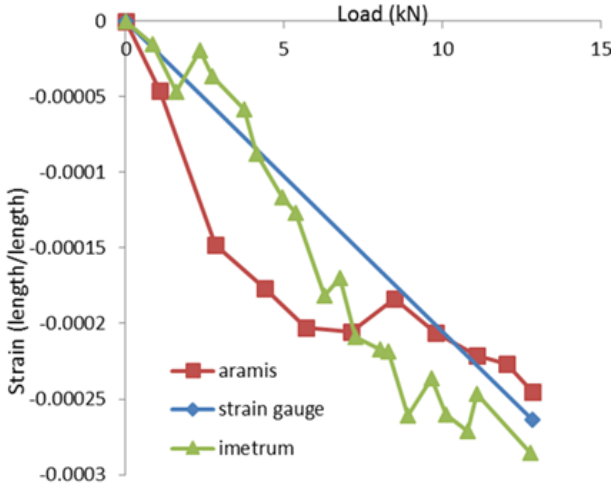

Figure 10. Comparison of Strains in the Middle of the Beam

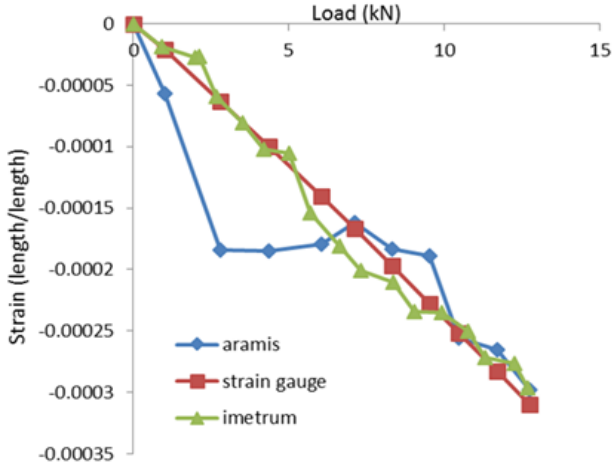

Figure 11. Comparison of Strains at the Bottom of the Joint

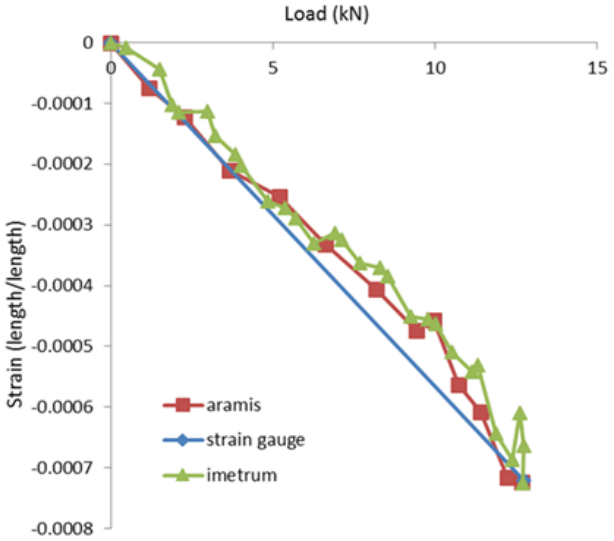

Figure 12. Comparison of Strains at the Bottom of the Beam

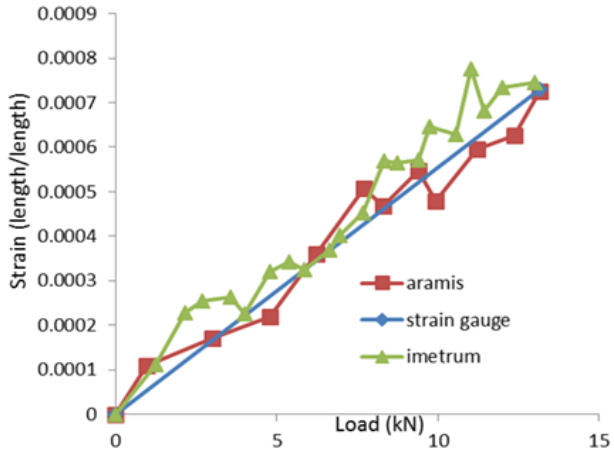

Figure 13. Comparison of Strains at the Top of the Beam

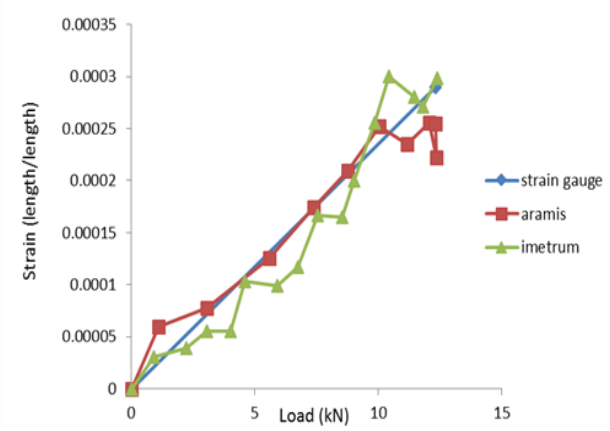

Figure 14. Comparison of Strains at the Top of the Joint

Based on the measured strain values, the accuracy of the DIC-based approach was determined for measuring strains lying within three ranges: 0-0.015% (by using the results in Figures 8 and 9); 0.015%-0.03% (by using the results in Figures 10, 11, and 14); and, 0.03%-0.075% (by using the results in Figures 12 and 13). R-squared (coefficient of determination) values were computed for each of the plots. At each strain gauge location, these values served as a measure of the closeness of the DIC-based strains to the straight-line model obtained via the strain gauge measurements. Since Figures 8 and 9 display strains having values in the range of 0-0.015%, of all the figures presented, they provided the most meaningful means for comparing strains having a value less than or equal to 0.015% (range 1 mentioned previously). While computing the R-squared values for the strains in ranges 2 and 3 discussed above, only those data points corresponding to strain values that lay within the range under scrutiny were considered in the R-squared computation. Consequently, the results in Figures 10, 11, and 14 were used to compare strains in the range of 0.015-0.03% by considering only those values of strain greater than 0.015%, and not considering strain values less than 0.015% in these figures.

Similarly, since the results in Figures 10, 11 and 14 were used to compare the strains in the range of 0.015%-0.03%, the values in Figures 12 and 13 were used to determine the accuracy of strains measured by the DIC-based approach for strains lying within the range of 0.03%-0.075% by considering only those strain values in Figures 15 and 16 greater than 0.03%, and not considering those values less than 0.03% in the R-squared value computation. Table 3 shows the R-squared values.

Discussion

1. The strain gauge responses showed a linear strain versus load behavior. This was due to the fact that the material was loaded within its elastic range of response.

2. In all of the figures presented (Figures 8-14), the strain versus load response obtained from the DIC-based ARAMIS and iMETRUM readings followed a general pattern, similar to the strain versus load response obtained using the strain gauges. Additionally, the maximum values of strain measured by the DIC-based approach were nearly identical to those measured by the strain gauges for strains in the range of 0.03%-0.075%. The percentage change between these maximum values (see Table 2, figures obtained by using the strain gauge value as the reference value) was most pronounced for strain measurements taken at the middle of the joint, with a difference of 44.82% in test 1 and 25% in test 2 using ARAMIS, and 47.65% and 46.21% using iMETRUM. This is reasonable, since the middle of the joint was the stiffest of all the locations investigated and developed the lowest strains in the specimen, on the order of approximately 0.015%. At locations that developed strains greater than 0.015%, and falling within the range of 0.015%-0.03%, the percentage changes between the maximum values measured by the strain

Table 3. R-Squared Values

Figure	Strain Range (%)	Type	R-squared ARAMIS	R-squared iMETRUM
8	0 – 0.015	compressive	0.5728	0.3772
9	0 – 0.015	compressive	0.7015	0.388
10	0.015 – 0.03	compressive	0.7382	0.8461
11	0.015 – 0.03	compressive	0.6827	0.98
12	0.03 – 0.075	compressive	0.9725	0.91
13	0.03 – 0.075	tensile	0.9716	0.8952
14	0.015 – 0.03	tensile	0.9252	0.9345

gauges versus those measured using the DIC-based approach predictably decreased and ranged from 3.56%-12.07% using ARAMIS and 2.91%-7.95% using iMETRUM. Finally, for even higher strains in range 3 (falling within the range of 0.03%-0.075%), the percentage change between peak strains measured using both approaches reduced to less than 0.7% in the case of ARAMIS and about 2% in the case of iMETRUM. Thus, purely from the perspective of peak strain computed by the DIC-based approach, it can be seen that this approach can accurately determine strains to a value of approximately 0.03% using both ARAMIS and iMETRUM, with the error in the peak strain measurement being less than 0.7% in the former case and no more than 2% in the latter.

3. Of all the comparisons shown in Figures 8-14, the most pronounced variation between the values of the strains obtained using the DIC-based approach versus the strain gauge values occurred in the middle of the joint (Figures 8 and 9). This is reasonable, since the middle of the joint was the stiffest of all the regions investigated and developed the lowest strains in the specimen, on the order of approximately 0.015%.

4. At the middle of the beam and the top and bottom of the joint (Figures 10, 11, and 14), where the peak strains fell within the range of 0.025%-0.03%, it can be seen that the strains measured by the DIC-based approach using ARAMIS resemble the strain gauge measurements more closely for strain values greater than approximately 0.015% (i.e., within the range of 0.015%-0.03%). This is reasonable since, based on the discussion in points 2 and 3, of all the locations studied in this investigation, the DIC-based approach was the least accurate for measuring strains less than 0.015%. However, in the case of iMETRUM, the strain measurements showed a greater resemblance to the strain gauge values for strains less than 0.015% in these plots than those shown by the ARAMIS values. Overall, in these plots, the pattern displayed by the iMETRUM strain resembled the pattern displayed by the strain gauge measurements and were better than the ARAMIS strains.

5. Figures 12 and 13 show the comparisons between the DIC-based strains and the strain gauge values for strains having a maximum value of approximately 0.073%. While interpreting these figures (see also point 6), it is meaningful to focus on the comparison of strains falling within the range of approximately 0.03%-0.075%, since the other figures focus on strains less than 0.03%. The peak strains in all figures, except for Figures 12 and 13, were within the range of 0.015%-0.03% and permitted a closer analysis and magnified view of strains of this order of magnitude.

6. The R-squared values presented in Table 3 were used as being representative of the accuracy of the DIC-based approach. These values lie between 0 and 1. A higher R-squared value implies a more accurate DIC-based strain measurement. The R-squared values obtained from Figures 12 and 13 were 0.9725 (at the bottom of the beam) and 0.9716 (at the top of the beam) for the ARAMIS measurements, and 0.91 and 0.8952 for the iMETRUM measurements at the same locations. As discussed in point 5, comparisons at these locations provide meaningful results for strains falling within the range of 0.03%-0.075%. Hence, it can be concluded that the DIC-based approach most accurately measured strains in the range of 0.03%-0.075%, to an accuracy of approximately 97% using ARAMIS, and about 90% using iMETRUM.

7. Comparisons at all of the other locations (other than the top and bottom of the beam) involved comparing strains that fell within the range of 0-0.03%. By subdividing this range into two smaller intervals, (0-0.015% and 0.015%-0.03%), it can be seen that the average R-squared value for the interval 0-0.015% was 0.6375 for the ARAMIS measurements and 0.3826 for the iMETRUM measurements. Additionally, the average R-squared value for the interval 0.015%-0.03% was 0.782 for the ARAMIS measurements and 0.9202 for the iMETRUM measurements. Hence, the DIC-based strain values were more accurate in the range of 0.015%-0.03% than they were in the range of 0-0.015%, which is reasonable, since the strain values in the former range are larger than those in the latter. Hence, it can be concluded that the DIC-based approach using ARAMIS does not produce accurate strain measurements for strains in both the 0-0.015% range (average R-squared = 0.6375) and 0.015-0.03% range (average R-squared = 0.782). Additionally, it can be concluded that the DIC-based approach using iMETRUM does not accurately measure strains less than 0.015% (average R-squared = 0.3826). However, for strains in the 0.015-0.03% range, the average R-squared values of 0.9202 obtained for the iMETRUM measurements leads to the conclusion that iMETRUM can be used to measure strains in this range to an accuracy of over 90%.

8. It can, therefore, be concluded that the minimum strain (in a region of a structure hidden from the na-

ked eye) that can be measured accurately by the DIC-based approach using the ARAMIS tool is 0.03%, and 0.015% for the iMETRUM tool is. This value of strain represents the minimum resolution of these systems in measuring strains.

Possible Causes of Error

1. Vibrations in the test specimen caused during manual load application: The strain readings computed using the DIC-based ARAMIS were very sensitive to any disturbances in the experimental specimen. Since the loads were applied manually, load application created vibrations in the specimen. Digital images were captured every 45 seconds in order to allow the specimen to settle and the vibrations to cease. However, it is possible that there were some vibrations, albeit negligible, in the specimen at the time of capturing the digital images. Measurements made using iMETRUM were less sensitive to the presence of specimen vibrations.

2. Vibrations in the test specimen due to external movement and disturbances in the lab (examples: other tests being conducted in the laboratory, large lab door being closed, people walking around, floor vibrations, etc.): While conducting the tests, it was observed that external vibrations created a significant fluctuation in the output strain readings obtained using the DIC-based ARAMIS. Despite attempting to create a highly controlled environment in order to minimize any external perturbations, it was not possible to completely isolate the specimen. Hence, small effects due to external vibrations could have marginally influenced the DIC-based strain measurements made using ARAMIS. The strain measurements made using iMETRUM were less sensitive to the presence of external vibrations in the vicinity of the test specimen.

3. During the calibration of the strain gauges, the mV output reading from the strain gauges was converted into a strain value by using a strain gauge factor of 2.13, provided by the supplier. It is possible that there were minor differences between the theoretical value and the real value. Hence, the strain gauge readings were not perfect.

4. Strain gauges were located on the rear surface of the specimen, and pictures were taken on the front surface in order to measure strains in the hidden region. Additionally, while using the software to compute the specimen strains (at the locations investigated in this study) after it processed the digital images, it was required to specify the location on the specimen's image on the software's graphical user interface at which the strain was desired. Since the strain gauges were located on the rear surface of the specimen, their exact location on the image could not be pinpointed with perfect accuracy. The strains were computed at locations that were very close to their exact locations. Small differences between the exact locations and the ones at which the strain values were obtained using the DIC-based tools could have caused minor variations between the strain gauge values and those obtained using the DIC approach.

5. While capturing the images, it was essential that the surface of the specimen being photographed was perfectly parallel to the camera surface. This was ensured at the start of the experiment. However, there was an extremely small movement of the specimen in the z direction, as the load was applied. This minute movement could have possibly introduced some minor error in the DIC-based calculations, since it resulted in the loss of the initial perfectly parallel orientation of the specimen surface with respect to the sensor surface.

6. The camera has to be placed perfectly parallel to the ground. Even a slight tilt can cause errors in the strain measurements.

Comparison between ARAMIS and iMETRUM

Vibrations of the specimen affected the ARAMIS measurements more than they did the iMETRUM measurements. Hence, it was easier to make these measurements using iMETRUM than it was using ARAMIS. iMETRUM made a continuous video recording of the deformation of the specimen as it was being loaded. This video recording served as the raw data that was processed by the DIC algorithms incorporated in the iMETRUM software. Vibrations existed in the specimen and were captured in the video recording. While processing the video recording, the iMETRUM algorithms filtered out the noise created by the specimen vibrations. While using ARAMIS, however, discrete digital images of the specimen captured at different stages of the loading process served as the raw data for the algorithms. There was a waiting period between the capture of consecutive images, because even the slightest disturbance in the specimen adversely affected the strain measurements produced by ARAMIS. Hence, considerable caution needed to be exercised during the performance of the test in the case of ARAMIS. This was not so in the case of iMETRUM. As

there was no waiting period between the application of load increments in the iMETRUM test, the duration of the test was also shorter than in the case of ARAMIS. The test took about 3-4 minutes in the case of iMETRUM and about 12-15 minutes in the case of ARAMIS. Since several tests were performed at each strain gauge location in order to obtain a consistent set of good results, this time difference was an important parameter. Finally, the measurements made using iMETRUM were not as sensitive to the intensity of the external light source as those made using ARAMIS. The only requirement was that the light needed to be applied uniformly across the specimen. In the case of the tests performed using ARAMIS, two light sources were used to brightly illuminate the specimen in order to obtain more accurate readings. iMETRUM can be used to make strain measurements in about one-third the amount of time as ARAMIS; it has a better minimum resolution in measuring strains than ARAMIS does (0.015% using iMETRUM versus 0.03% using ARAMIS); it is easier to use and does not require the user to be as sensitive to perturbing the specimen as ARAMIS does; and, it can be used to make measurements under the effect of a light source of lower intensity than is needed by ARAMIS.

Summary and Conclusions

Damage observed in the connections of the Storstrom Bridge in Denmark was hidden from the naked eye and, hence, was not appropriately addressed at its onset, leading to its propagation. Identification of such damage at its onset can prevent its spread, thereby saving money and time on repairs, and also increasing the safety of the structure. Thus far, DIC-based SHM techniques have been used to monitor the structural condition of bridges on a global scale (for example, by measuring global deflections of bridges). In doing so, local damage such as that observed in the Storstrom Bridge can go undetected. Consequently, in this investigation, the DIC technique was applied in analyzing the strains of a small, localized region (a beam-to-column connection) of the Storstrom Bridge hidden from the naked eye (behind the gusset plates), and the lowest possible strains that could be accurately measured using this methodology were determined.

A beam-to-column connection in the Storstrom Bridge was replicated in the laboratory and subjected to a progressively increasing load that produced a shear force and bending moment at the connection. The strains that developed in the connection were measured using state-of-the-art DIC-based ARAMIS and iMETRUM tools, and were compared with the strains measured using strain gauges as a reference. It was determined that the DIC-based ARAMIS and iMETRUM tools can accurately measure strains as low as 0.03% and 0.015%, respectively. Due to the challenges faced in making these small-strain measurements with ARAMIS, even under highly controlled laboratory conditions, it was concluded that it is currently unrealistic to use ARAMIS in a real-world situation to measure strains as small as those that would need to be measured in order to detect the onset of damage in bridge connections. The strain measurements made using iMETRUM were less sensitive to the presence of vibrations created in the specimen, due to external moving loads. Consequently, in order to determine whether it is realistic to use iMETRUM in a real-world scenario involving the presence of vibrations in the structure being monitored that are produced by external moving loads, additional work needs to be done where the minimum strain that can be measured using iMETRUM is determined when the specimen is subjected to external vibrations.

References

[1] Kaphle, M., Tan, A., & Thambiratnam, D. (2009). Structural health monitoring of bridges using acoustic emission technology and signal processing techniques. *Proceedings of the 13th Asia Pacific Vibration Conference*, New Zealand.

[2] Ahlborn, T. M., Shuchman, R., Sutter, L., Brooks, C., Harris, D., Burns, J., et al. (2010). *The State-of-the-Practice of Modern Structural Health Monitoring for Bridges.* Report prepared at the Department of Civil and Environmental Engineering, Michigan Tech Transportation Institute, Michigan Technological University, Houghton, Michigan.

[3] Gentile, C., & Bernardini, G. (2010). An interferometric radar for non-contact measurement of deflections on civil engineering structures: laboratory and full-scale tests. *Structure and Infrastructure Engineering*, *6*(5), 521-534.

[4] Desai, N. (2016). Small-Strain measurement in bridges using the digital image correlation (DIC) technique. *Proceedings of SPIE 9805, Health Monitoring of Structural and Biological Systems* (980530).

[5] Winkler, J., Fischer, G., & Georgakis, C. T. (2012). Localized bending fatigue behavior of high-strength steel monostrands. *Proceedings of the 6th International Conference on Bridge maintenance, Safety and Management* (IABMAS), Italy.

[6] Winkler, J., Fischer, G., & Georgakis, C. T. (2012). Monitoring of localized deformations in high-strength steel cables. *Proceedings of the. NDE/NDT for Highways and Bridges: Structural Materials Technology (SMT) 2012 Conference*, New York, USA.

[7] Jiang, R., Jauregui, D. V., & White, K. R. (2008). Close-range photogrammetry applications in bridge measurement: Literature review. *Measurement: Jour-*

nal of the International Measurement Confederation (IMEKO), *41*, 823-834.
[8] Perez, L. S., Fischer, G., & Georgakis, C. T. (2012). *Determination of Localized Strains and Global Deformations Using Video System*. Master's Thesis, Technical University of Denmark, Kgs. Lyngby, Denmark.
[9] Lin, G., Tan, H., & Wang, C. (2008). Pressure Airship Model Structural Analysis and Deformation Measurement Using Photogrammetry. *Proceedings of the International Conference on Experimental Mechanics*, Nanjing, China.
[10] Lee, T. K., & Al-Mahaidi, R. (2008). An experimental investigation on shear behaviour of RC T-beams strengthened with CFRP using photogrammetry. *Composite Structures, 82*, 185-193.
[11] Jauregui, D. V., White, K. R., Woodward, P. E., & Leitch, K. R. (2003). Noncontact Photogrammetric Measurement of Vertical Bridge Deflection. *Journal of Bridge Engineering, 8*(4), 212-222.
[12] Waterfall, P. M., Macdonald, J. H. G., & McCormick, N. J. (2012). Targetless precision monitoring of road and rail bridges using video cameras. *Proceedings of the 6th International Conference on Bridge maintenance, Safety and Management* (IABMAS), Italy.
[13] Busca, G., Cigada, A., Mazzoleni, P., Zappa, E., & Franzi, M. (2012). Cameras as displacement sensors to get the dynamic motion of a bridge: performance evaluation against traditional approaches. *Proceedings of the 6th International Conference on Bridge maintenance, Safety and Management* (IABMAS), Italy.
[14] Yarnold, M. T., Moon, F. L., Aktan, A. E., & Glisic, B. (2012). Structural monitoring of the Tacony-Palmyra Bridge using video and sensor integration for enhanced data interpretation. *Proceedings of the 6th International Conference on Bridge maintenance, Safety and Management* (IABMAS), Italy.
[15] Furlan, M. (2014). *Use of Digital Image Correlation for Steel section Strain Evaluation*. Master's Thesis. Supervisors: Dr. Christos Georgakis and Dr. Claudio Modena.

Biographies

NIRANJAN DESAI is an assistant professor of civil engineering at Purdue University Northwest. His areas of research interest include structural health monitoring and nonlinear dynamic analysis. In 2014, he was awarded the "Alan Yorkdale Memorial Award" for his journal paper titled "*A study of the out-of-plane performance of brick veneer wall systems in medium rise buildings under seismic loads.*" Dr. Desai may be reached at desai39@pnw.edu

CHRISTOS GEORGAKIS is a full professor in the Department of Civil Engineering at the Technical University of Denmark and Head of the Civil Engineering Structural Dynamics Group, CESDyn. CESDyn is a research-oriented group working in the field of civil engineering structural dynamics. Research activities are mainly based on experimental work investigating the effect of environmental loading on structural response. Core areas are wind loading in general, additional effects due to rain, snow and ice accretion, seismic loading, and the impact of human-induced vibration. Christos Georgakis has published 16 journal articles in structural dynamics and vibration control and is co-author of the book *Cable Supported Bridges: Concept and Design*, in which he authored the chapter on monitoring of bridge structures. Dr. Georgakis may be reached at cg@byg.dtu.dk

GREGOR FISCHER is an associate professor in the Department of Civil Engineering at the Technical University of Denmark. Dr. Fischer may be reached at gf@byg.dtu.dk